ELSEVIER

Tectonophysics 297 (1998) 31–50

TECTONOPHYSICS

Thermal effects of exhumation of a metamorphic core complex on hanging wall syn-rift sediments: an example from the Rechnitz Window, Eastern Alps

István Dunkl [a,b,*], Bernhard Grasemann [c], Wolfgang Frisch [a]

[a] *Institut für Geologie und Paläontologie, Universität Tübingen, Sigwartstrasse 10, D-72076 Tübingen, Germany*
[b] *Laboratory for Geochemical Research, Hungarian Academy of Sciences, Budaörsi út 45, H-1112 Budapest, Hungary*
[c] *Institut für Geologie (Geozentrum), Universität Wien, Althanstrasse 14/2B447, A-1090 Vienna, Austria*

Received 19 March 1997; accepted 29 September 1997

Abstract

The removal of overburden by tectonic processes displaces the rock masses and their temperature with respect to the surface. Consequently high cooling rates and increased heat flow have been reported from rapidly exhuming terrains. Previous studies were mainly focused on the greenschist- and amphibolite-facies tectono-thermal evolution of the footwall. A two-dimensional numerical thermal model presented in this study concentrates on the thermal history of the hanging wall and the footwall blocks and evaluates the variation of the near-surface heat flow above an evolving metamorphic core complex. Based on structural, thermobarometric and geochronological constraints from the Rechnitz core complex of the Eastern Alps the modelling suggests that rapid movement along the extensional fault took place between 22 and 17 Ma. During this period the heat flow reached values of 140–150 mW/m^2 in the hanging wall in a 10–15-km-wide zone parallel to the fault trace. The increased heat flow caused the high coal rank in the Miocene syn-rift sediments deposited on the hanging wall. Apatite fission track geochronology of the thermally overprinted sedimentary deposits gives the time at which the bottom of the syn-rift sediment pile passed through 110ºC (13.6 $\pm$ 0.9 Ma). The vitrinite reflectance data (R_r: 0.67–1.04%) suggest significant burial of the margin of the hanging wall at the time of core complex formation. Considering the coal rank data and the thermal conductivity of the sedimentary deposits by modelling of the organic maturation we calculate syn-rift (Early–Middle Miocene) burial of the hanging wall margin of the Rechnitz core complex to be 1100–1600 m. This value shows the importance of the post-Middle Miocene erosion of the region, which was related to the inversion of the Pannonian basin.

Keywords: Alps; Neogene; fission-track; core complex; finite-element analysis; thermal maturity

1. Introduction

The Styrian basin is a southwestern marginal depression of the Pannonian basin system (Fig. 1), which was formed during Miocene extension (Royden et al., 1983). Vitrinite reflectance studies of the Styrian basin show a complex pattern of coal maturity in the Neogene basin fill (Sachsenhofer, 1990, 1991, 1992; Ebner and Sachsenhofer, 1991a,b). Evaluation of the maturity parameters and modelling of the thermal history shows that heat flow was in-

* Corresponding author. Fax: +49 7071 5059; E-mail: dunkl@uni-tuebingen.de

0040-1951/98/$19.00
PII: S0040-1951(98)00162-0

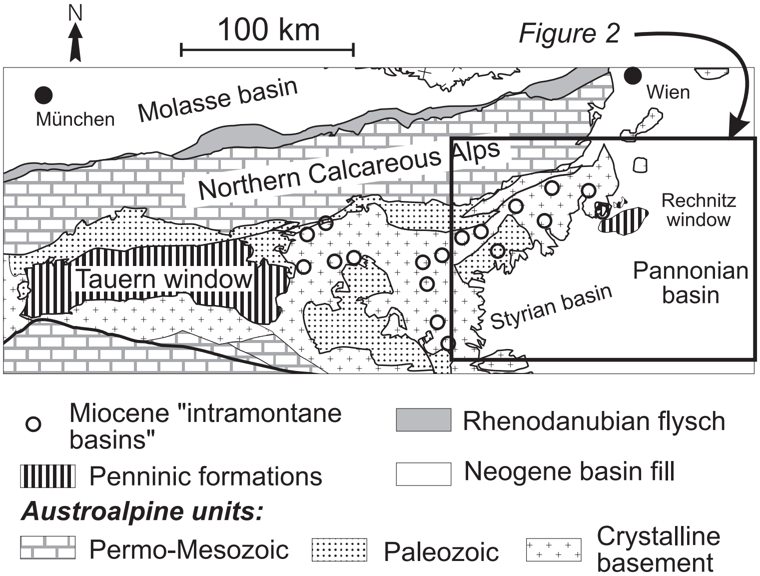

Fig. 1. Sketch map of Eastern Alps.

creased during Early–Middle Miocene times (Sachsenhofer, 1992, 1994). In the central part of the basin near the volcanic centres the coal rank is strongly increased (up to 3.5% R_r). At the southwestern and northeastern margins of the Styrian basin, in a few kilometres wide belt along the crystalline basement, the coalification of the sediments also shows a post-depositional overprint. However, there is no evidence for volcanic activity and therefore there is no obvious relation between the unexpectedly high vitrinite reflectance (up to 1.04% R_r) and subvolcanic bodies.

The interpretation of the maturity of the Miocene syn-rift sediments in the border zone between the Eastern Alps and the Pannonian basin is controversial since the original publications of Sachsenhofer (1991) and Ebner and Sachsenhofer (1991a). The sediments were deposited in an extensional zone in the vicinity of the Penninic Rechnitz Window, which opened during the Miocene as a metamorphic core complex by tectonic denudation of the Austroalpine nappe complex (Tari and Horváth, 1995; Fig. 1). As the Styrian basin to the southwest of this metamorphic core complex contains prominent volcanic edifices (Fig. 2), the first and most obvious explanation of the coal rank values was to relate them to the increased heat flow from a subvolcanic body (Belocky et al., 1991). The epithermal stibnite mineralisation that deposited in veins in the Penninic rocks was supposed to be also related to a hidden intrusive body. However, there are no volcanic formations close to the sample sites of our study (Grum et al., 1992; see Fig. 2).

Fission track dating was carried out on detrital apatite and zircon crystals to clarify the post-depositional thermal history of the Neogene sediments. Numerical thermal modelling was completed in order to evaluate the thermal history and near-surface heat flow in the hanging wall during core complex formation.

2. Geology

Along the central axis of the Eastern Alps several tectonic windows contain Penninic units. The study area is situated close to the easternmost Penninic exposure, the Rechnitz Window (Fig. 2). The Rechnitz Window and the 'Rába River extensional corridor' (Tari, 1994) were formed in the Middle Miocene during the orogenic collapse of the Eastern Alps (Pahr, 1980; Ratschbacher et al., 1989, 1990; Tari and Horváth, 1995; Decker and Peresson, 1996; Dunkl and Demény, 1997). Fault-scarp-related coarse debris was deposited as basin formation began in the Middle Miocene (Herrmann and Pahr, 1988). The Sinnersdorf formation includes

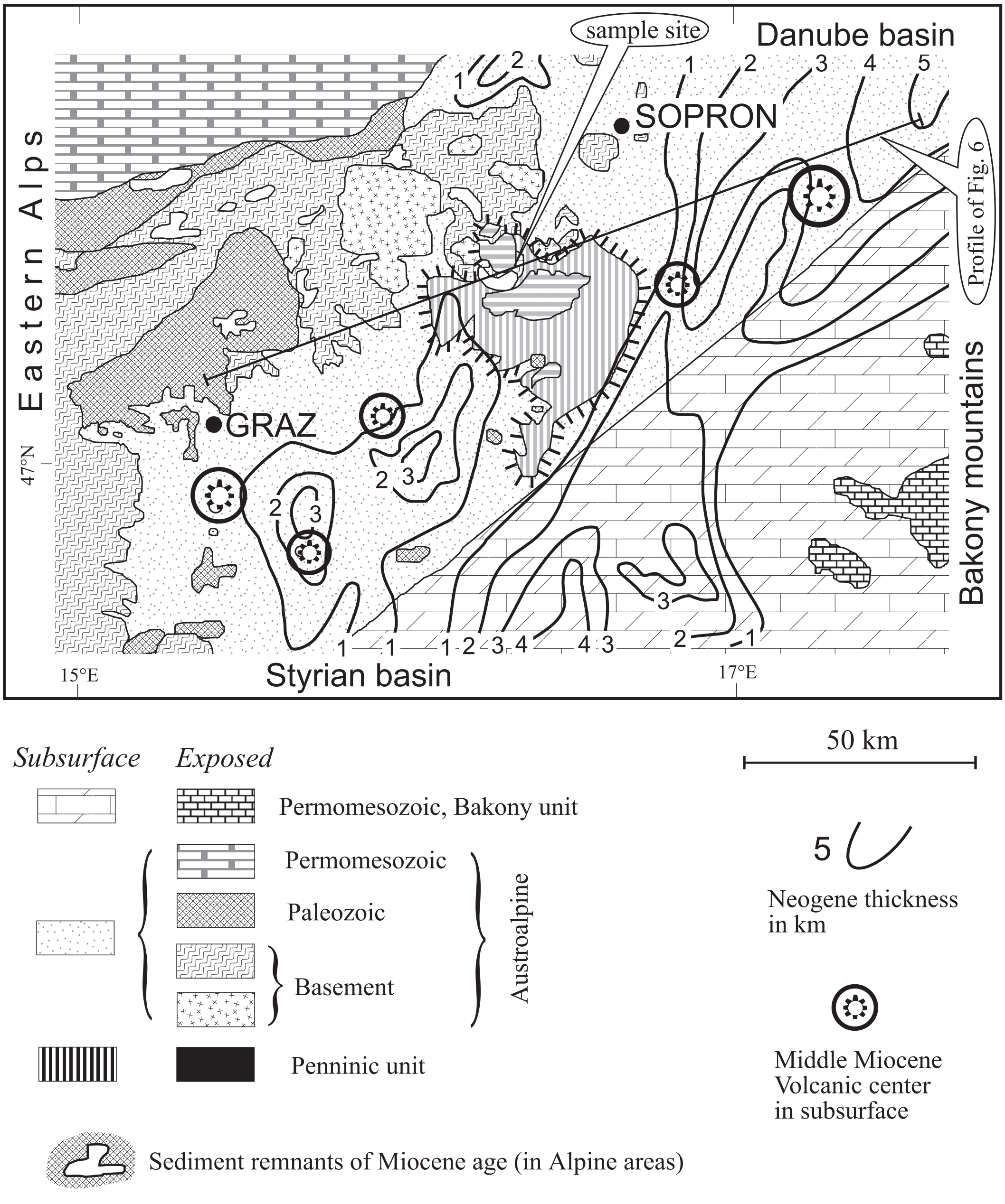

Fig. 2. Simplified geological map of the study area (after Flügel and Neubauer, 1984; Horváth, 1985; Fülöp and Dank, 1987; Flügel, 1988; Tari and Horváth, 1995).

very coarse components at the base of the sequence (boulder size up to 22 m). The age of the beginning of deposition is poorly documented by fossils, but in analogy to similar occurrences elsewhere, is considered to be Ottnangian–Karpatian (19–16.5 Ma; Paratethyan timescale according to Steininger et al., 1988). The fanglomerate- and conglomerate-dominated basal sequence is covered by a sandy, silty and marly sequence with coal bands. The sediment was deposited on the hanging wall of the metamorphic core complex and does not contain any material derived from the footwall (from the Penninic formations). The detrital components are only gneiss and micaschist pebbles and finer debris of these lithologies, derived from the Austroalpine nappe complex. Epidote —the most characteristic detrital mineral of Penninic rocks— appears in sediments at the end of Sarmatian time (<12 Ma; Pahr, 1984).

Along the western side of the core complex subsidence was moderate. However, northeast of the structure (where the lid of the window was removed) the continuing continental extension created deep basins in Late Miocene time (up to 6 km sediment fill; see Fig. 2). Such asymmetry is typical for metamorphic core complexes (Reynolds and Lister, 1990). In the vicinity of the core complex the sediment sequence was later deeply eroded and only thin basal members have been preserved as irregular-shaped basin remnants.

3. The aim of the heat flow modelling

Many studies of the thermal evolution of metamorphic core complexes have been focused on the exhumation and cooling history of the footwall (e.g. Dokka et al., 1986; Davis and Lister, 1986; Ruppel et al., 1988; House and Hodges, 1994; Lachenbruch et al., 1994; Ketcham, 1996). However, rapid exhumation of the footwall along normal faults together with advection of heat can cause heating of the adjacent hanging wall (Grasemann and Mancktelow, 1993). Thus the temperature history of the hanging wall represents important insights to tectonic movements (Fayon et al., 1996). This process is shown in Fig. 5, in which theoretical cooling curves for a sample located at shallow depth within the hanging wall and for a sample being exhumed from a deeper position within the footwall during normal faulting are plotted. The grey area represents the period of main tectonic movement along the normal fault where the exhumation rate of the footwall is assumed to be rapid (i.e. >1 mm/a). During rapid movement, the footwall shows a convex upwards shape because of the increase of the geothermal gradient due to advection of heat. After the cessation of rapid movement, the cooling curve changes its shape to a concave-upwards form because of the relaxation of the increased geothermal gradient. Consequently, the change from the steep to the flat part of the curve (i.e. from fast to slow cooling) *does not coincide* with the transition from high to low exhumation rates in the footwall. This change in tectonic movement is rather recorded near the inflexion point where the shape changes from convex upwards to concave upwards. If the effect of advection of heat in the footwall is strong enough the hanging wall warms up due to the rise of the geothermal gradient (van Wees et al., 1992; Grasemann and Mancktelow, 1993; Fayon et al., 1996). The importance of this process is clearly a function of the displacement rate of the detachment and the fault dip angle (Buck et al., 1988). It is very important to note that the temperature peak in the hanging wall *coincides* with the transition from high to low exhumation rates in the footwall. Whether this temperature peak in the cooling curve represents an absolute or local maximum depends on whether the hanging wall experienced subsidence or exhumation.

The main aim of the numerical thermal modelling is to use thermal, tectonic and geometric parameters constrained by local and regional geological observations and to quantify the amount of temperature rise or, more exactly, the amount of near-surface heat flow within the hanging wall immediately above the Rechnitz metamorphic core. These values will be reentered in a coal maturation modelling program in order to estimate the thickness of the syn-rift sediments in the hanging wall.

Note, that numerous processes can influence the lateral distribution of the near-surface heat flow including igneous activity, thermal disturbance by moving water, heat production by radioactive elements or frictional heating (Sass et al., 1994). However, in regions of high tectonic activity and exhumation the transport of heat by moving rocks is clearly the first-order effect that is the central interest of this study.

4. Fission track results

Zircon and apatite fission track (FT) geochronology was carried out on Early Miocene siliciclastic sediments deposited on the hanging wall of the Rechnitz Window. A part of these deeply eroded basin

Table 1
Fission track results from the Penninic rocks of the Rechnitz Window

Code	Locality	Petrography	Cryst.	P_s	(N_s)	P_i	(N_i)	$p(\chi^2)$ (%)	Peak age	Pooled age (Ma $\pm$ 2σ)
Apatite ages										
KRA-7	Lockenhaus	fanglomerate	54	1.12	(1071)	8.35	(8128)	<1	11.9	13.3 ± 1.2
KRA-9	Goberling	sandstone	40	1.66	(777)	12.7	(5891)		11.1	12.8 ± 1.2
KRA-10	Goberling	conglomerate	45	1.59	(794)	10.4	(5276)	1	12.3	14.8 ± 1.4
KRA-12	Goberling	sandstone	38	1.85	(975)	13.8	(7250)	<1		13.5 ± 1.2
All data					(3617)		(26545)	–	11.2	13.6 ± 0.9
Zircon ages										
KRA-7	Lockenhaus	fanglomerate	47	100.6	(5268)	35.4	(1798)	2	58	58.8 ± 5.1
KRA-9	Goberling	sandstone	38	75.6	(3012)	29.1	(1149)	<1	45	52.7 ± 5.1
KRA-10	Goberling	conglomerate	50	80.1	(4407)	33.0	(1829)	<1	45	49.8 ± 4.3
KRA-12	Goberling	sandstone	39	75.1	(3591)	31.0	(1489)	5	46.2	49.7 ± 4.5
All data					(16278)		(6265)		47.4	53 ± 3.9

Track densities (P) are as measured and are ($\times 10^5$ tr/cm^2); number of tracks counted (N) shown in brackets, $p(\chi^2)$ is probability of obtaining χ^2 value for n degree of freedom (where n = no. crystals-1), apatite ages calculated using dosimeter glass SRM 612 with zeta $= 373 \pm 8$; zircon ages calculated using zeta $= 370 \pm 11$.
s = spontaneous; i = induced.

ruins shows post-depositional thermal overprint. In these localities the vitrinite reflectance ranges between 0.67 and 1.04% R_r, while in other occurrences of synchronous Miocene sediments the R_r values are around 0.4% (Belocky et al., 1991). Such an overprinted basin fragment was investigated to obtain fission track samples derived from the basin floor immediately above the main detachment of the core complex.

The analytical method is described in Appendix A, the localities, lithologies and measured FT ages are listed in Table 1. There are no significant age differences between the ages of the samples, both zircon and apatite results are consistent.

The zircon FT ages gave a mean in Early Eocene time, which is clearly pre-depositional. Although the chi-square tests fail, the shape of the age spectra are symmetric and rather narrow indicating a single source for the detrital minerals (Fig. 3). This is in accord with the local provenance and the very short transport of the detritus. The coarsest sediment (KRA-7, derived from the very bottom of the sequence) gave the oldest age, because at the beginning of Miocene sedimentation the top of the zircon partial annealing zone was eroded. Zircon FT ages are generally 15–20 million years younger than the main cluster of mica K/Ar ages in the surrounding Austroalpine basement (~80 Ma; Müller et al., 1992). The zircon FT datum can be due to a late stage of a long-lasting post-Cretaceous cooling or to an independent Tertiary exhumation event of the Austroalpine pile.

The apatite FT ages are younger than the age of sedimentation, as the post-depositional thermal overprint annealed the pre-existing tracks. The age spectra are mainly symmetric (the irregularity of KRA-12 is probably due to the lower number of usable grains). For the characterisation of the crystal populations the pooled-ages are more reliable than the peak-ages, as (1) the high coal rank (0.67–1.04% R_r) proves total resetting and the FT ages of the grains are therefore independent of their provenance, and (2) the peak-ages are biased, being consistently younger than the mean. The average of the data is 13.6 Ma. This datum is interpreted as rapid cooling, because there are no strongly shortened tracks: the length distribution is narrow (Fig. 4), with average and standard deviation similar to fast cooled volcanic rocks (Fig. 5).

5. Review of the input parameters for modelling

5.1. Pressure–temperature conditions of the footwall before exhumation

Polymetamorphic oceanic sediments of Mesozoic age are exposed in the footwall of the Rechnitz core

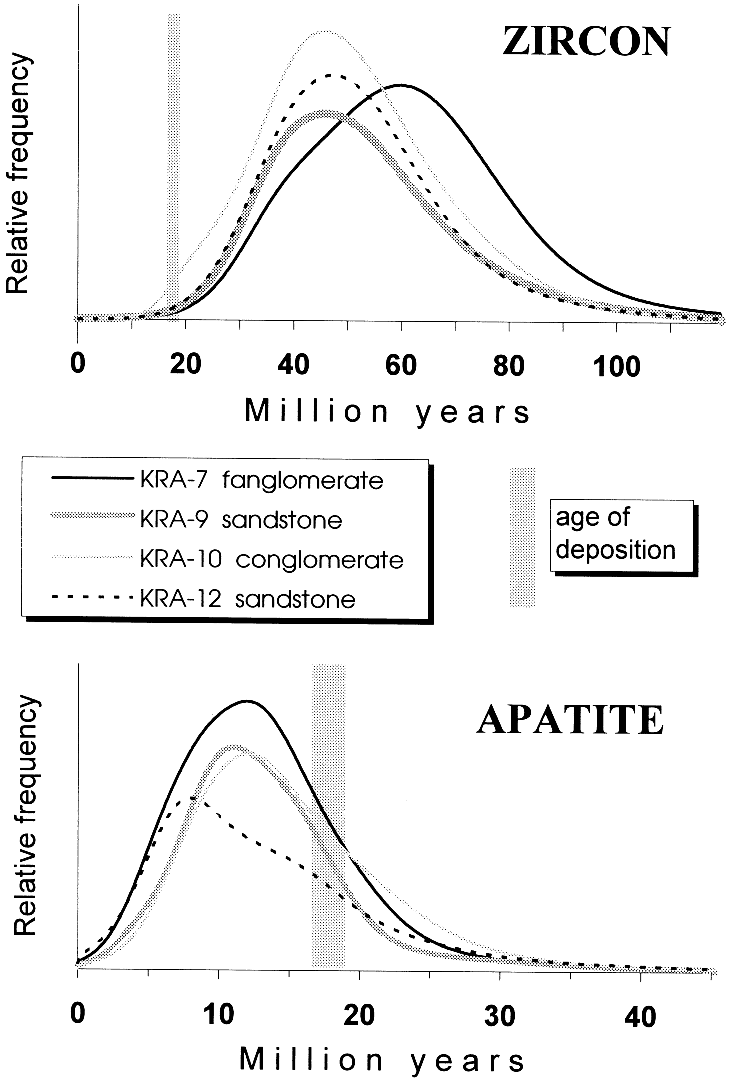

Fig. 3. Age spectra of the samples (calculated by the method of Hurford et al., 1984).

complex (Schönlaub, 1973). Quartz-, and carbonate-phyllite, greenschist, serpentinite, metaconglomerate and metagabbro are the predominant rock types. Three metamorphic events have been recorded: (1) oceanic hydrothermal activity; (2) subduction-related HP/LT metamorphism; and (3) late Alpine greenschist-facies metamorphism. Koller (1985) determined the temperature range for the latest metamorphism with 350°C to 430°C and the pressure with 3 kbar. The resetting of the white mica K/Ar ages at around 20 Ma also implies a minimum temperature of 350°C (W. Frank, pers. commun., 1992). Based on these *PT* conditions we assume a minimum initial depth of the exposed part of the footwall of 10 km at the beginning of the Miocene tectonic denudation process.

5.2. Timing of extension

It is difficult if not impossible to determine the beginning and duration of continental extension from the record of the Rechnitz Window alone. This win-

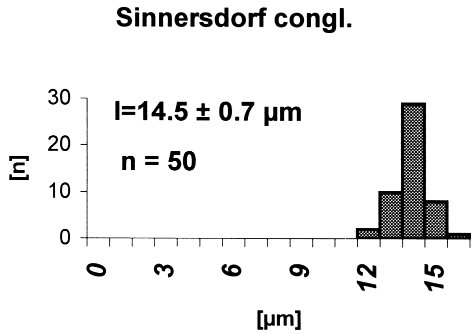

Fig. 4. Confined track length distributions in KRA-7 apatite sample.

dow is only a local manifestation of the Neogene stretching event affecting the entire Eastern Alps (Ratschbacher et al., 1991). For a proper evaluation we have to consider all of the relevant geochronologic data from the entire region in conjunction with the sedimentary record and the structure of the western Pannonian basin as documented by seismic studies.

Rapid subsidence and sedimentation in the intramontane basins east of the Tauern Window and the Styrian basin started in Ottnangian/Karpatian times (19–16.5 Ma). Although the palaeontological record is rather uncertain, the synchronous start of sedimentation in different basins over a large area is considered proof of an important extension event in the Eastern Alps.

Ratschbacher et al. (1989) suggest an age of 20 Ma (Early Miocene) for the beginning of continental escape for the Eastern Alps. Tari et al. (1995) also postulated the age of the large-scale displacements as Early Miocene (21–17 Ma). Apatite fission track data cluster around 20 Ma from the zone of the Periadriatic lineament (I. Dunkl, unpubl. results).

Zircon fission track ages from the exposed part of the Rechnitz Window range from 22 to 13.4 Ma with an average of 17.3 Ma (Dunkl and Demény, 1997). These ages indicate that the exhumation of the Penninic unit had initiated by Early Miocene time.

White mica Rb/Sr and amphibole Ar/Ar studies of the eastern Tauern Window have proven that the thermal peak of the metamorphism was attained between 30 and 24 Ma (Cliff et al., 1985; Inger and Cliff, 1994). In the western Tauern Window the climax is younger, and in the central part older (~20 Ma and 36–32 Ma, respectively; Blanckenburg et al., 1989; Zimmermann et al., 1994). A well pronounced cluster of mica cooling ages around 18–

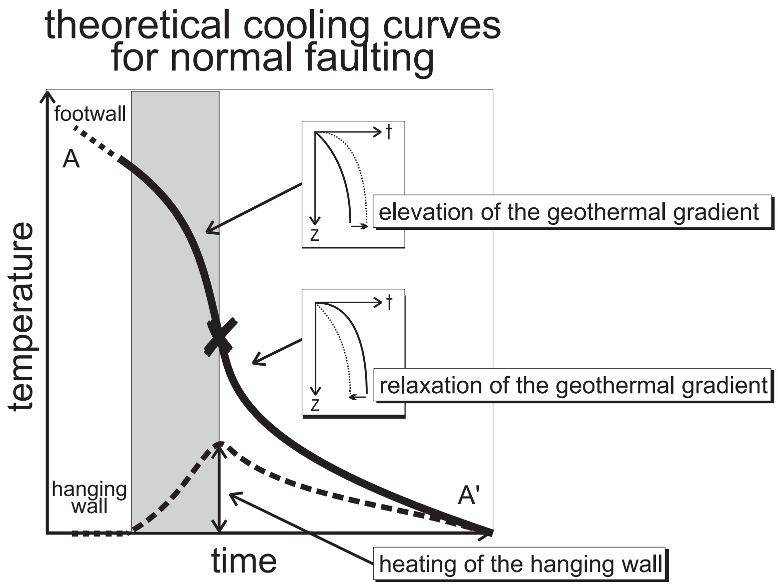

Fig. 5. Theoretical cooling curves for the hanging wall and footwall during normal faulting. The shaded region indicates a period of rapid movement. Due to the elevation of the geothermal gradient and the subsequent relaxation the cooling continues after the cessation of rapid movement.

16 Ma indicates acceleration of the cooling (Cliff et al., 1985). The extension rate was probably highest during this period.

The termination of extension in the Pannonian region was considered by Royden et al. (1983) to be as young as the Sarmatian/Pannonian boundary (11.6–12 Ma). Re-interpreting numerous seismic lines, Tari (1994) placed the boundary of syn-rift/post-rift tectonics in the Pannonian basin at the end of the middle Badenian (~13.8 Ma). This datum is in good agreement with the reset apatite FT ages reported in this paper (average: 13.6 ± 0.9 Ma). A third (independent) deduction of the timing was made by Sachsenhofer (1994), who concluded that the period of increased heat flow lasted from 17 to ~12 Ma, based on his modelling of the organic maturation data of the central part of the Styrian basin.

We conclude that the maximum duration of the extension process was possibly as long as 10 million years. But the well documented, most pronounced interval with high extension rates was only 4–5.5 Ma long.

5.3. Geometry of exhumation

The low-angle normal faulting dominated tectonic denudation was accompanied by strike-slip movements (Ratschbacher et al., 1990). The extension was approximately ENE–WSW oriented, so the cross-section and the modelling section are also oriented

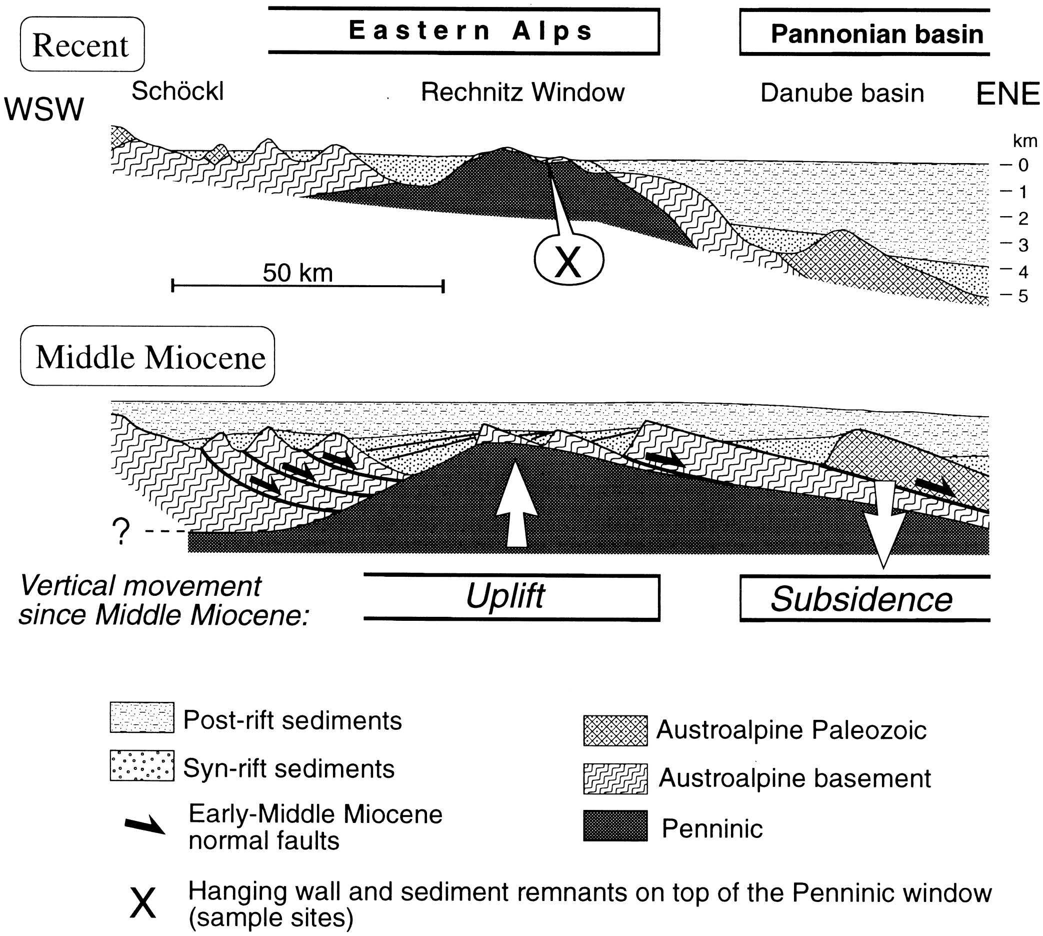

Fig. 6. Strike section across the Rechnitz Window (position is in Fig. 2). First panel: recent situation; second panel: burial in Late Miocene. White arrows indicate the late stage uplift of the core complex and the subsidence of the Danube basin. This subsidence was related to the final, wide rift and narrow rift stages of extension, during the Late Miocene (Tari and Horváth, 1995).

in this direction (Fig. 6). The internal structure of the Danube basin (Fig. 2) is well known, due to intense seismic research (Tari, 1994), but sporadic outcrop observations of the ductile and brittle fabrics exist only from the western side of the core complex. The only available E–W seismic profile from the Eastern Alps is rather diffuse and does not show the top and the internal structure of the Penninic unit (Aric et al., 1987). Lack of data permits only speculation about the angle and depth of the detachment. Restoring the Miocene geometry the following facts have to be considered: (1) the recent angle of the detachment is very shallow; (2) ENE-directed ductile flow prevailed in the Penninic unit (Ratschbacher et al., 1990); (3) Tari (1994) considered the total extension of the structure to be around 80 km; (4) the hanging wall suffered radical thinning around the window (Tari, 1994), and the Austroalpine flakes on top of the Penninic dome are only remnants of thinned and tilted blocks (see Fig. 6); (5) the main detachment of the core complex is situated immediately below the studied sediments, the thickness of the slab ruins of the Austroalpine lid is 200–250 m at the most; (6) the cooling rate of the Penninic rocks was fast during Early and Middle Miocene times (40–50ºC/Ma; Dunkl and Demény, 1997); (7) there is moderate younging of the zircon FT cooling ages from west to east within the window (Dunkl and Demény, 1997); (8) there is a jump in the radiometric ages at the boundary of the window; mica K/Ar and zircon FT ages cluster around 80 and 60 Ma, respectively, in the Austroalpine (hanging wall) unit, while in the Penninic unit (footwall) these geochronometers yield ages around 21 and 17 Ma (Müller et al., 1992; Dunkl, 1992).

The main detachment was considered by Neubauer and Genser (1990) and Ratschbacher et al. (1991) as a continuous plane between the Tauern Window and the Rechnitz Window separating the Austroalpine and the Penninic units. For structural and tectono-stratigraphic reasons Tari (1994) put the main detachment into the Austroalpine pile. However, the jump of both the zircon FT and the mica K/Ar ages between the Austroalpine and Penninic units at the margin of the Rechnitz Window proves that the detachment in fact is located at the Austroalpine/Penninic boundary at the present erosion level. The same is true for the large parts of Tauern Window.

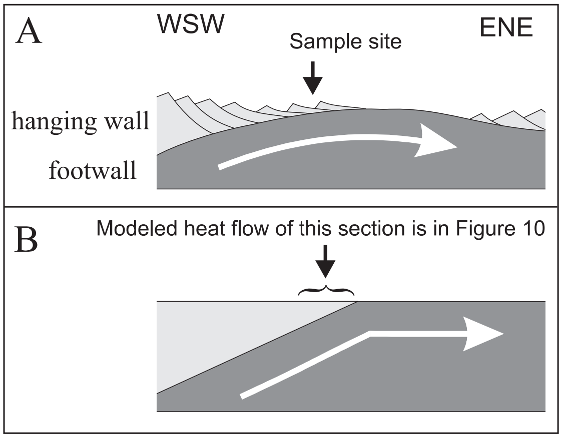

Fig. 7. Schematic section across the assumed original geometry (A) and the modelled geometry (B).

The original dip of the detachment faults is a crucial question in the interpretation of core complexes (John, 1987; Buck et al., 1988; John and Foster, 1993; Dokka, 1993; Buck, 1993). In the case of the Rechnitz Window Tari (1994) assumed an originally planar low-angle normal fault of 6–7º inclination. However, geochronological data suggest that the main detachment had to be formed at a steeper angle. The high cooling rates require upward movement of the footwall along high-angle normal faults. This problem can be explained by (1) an original ramp–flat–ramp geometry, or (2) by a rolling hinge mechanism. In the second case the detachment was planar with relatively high dips in the deeper part and has become subhorizontal only at the final exhumation of the footwall (Wernicke and Axen, 1988; Buck et al., 1988; Bartley et al., 1990). In the presented model the originally curvilinear displacement path of the footwall of the core complex has a more simple geometry (Fig. 7).

6. Numerical thermal modelling

Based on the geological observations discussed above, the following simplified geometry, initial conditions, boundary conditions and parameter configuration were chosen for the numerical model (see Fig. 8; Table 2; Appendix B). It is important to emphasise that the numerical modelling uses extremely simplified geometric and physical conditions. Never-

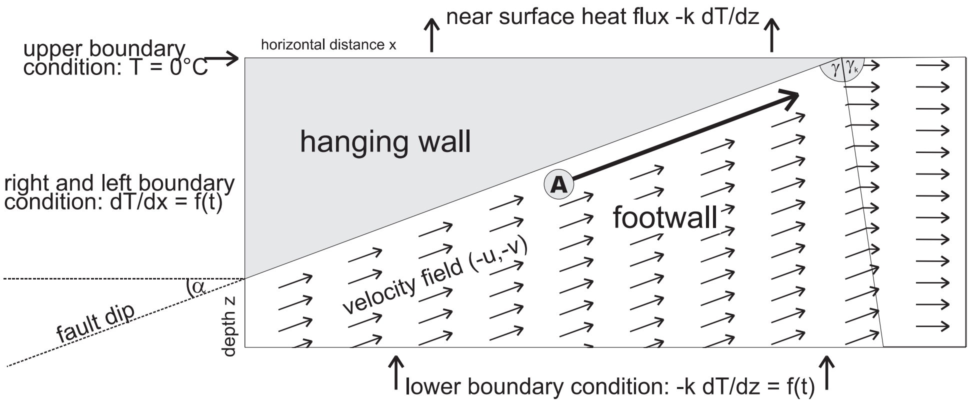

Fig. 8. Cartoon of the geometry and boundary conditions of the numerical model for normal faulting. During footwall exhumation the temperature and location of the observed rock sample *A* is recorded and compared with the thermochronological data (see Fig. 9). After the period of rapid exhumation the near-surface heat flow is measured and plotted in a parameter map (Fig. 10).

theless the most important boundary conditions that influence the near-surface gradient are considered. Furthermore, one-dimensional solutions — neglecting lateral cooling during normal faulting — put an upper limit on the estimates of surface heat flow.

Table 2
Physical parameters used for analytical and numerical calculations

Symbol	Description	Constant/unit
T	temperature	(K)
T_s	surface temperature	273 (K)
	temperature at base of lithosphere	1573 (K)
Δt	finite time step	10,000 (a)
	duration of rapid movement	5 (Ma)
	duration of slow movement	17 (Ma)
κ	thermal diffusivity	10^{-6} (m^2/s)
C	specific heat	1100 (J kg^{-1} K^{-1})
ρ	density	2800 (kg/m^3)
k	conductivity	3.08 (W m^{-1} K^{-1})
q_m	mantle heat flux	variable (W/m^2)
A_0	heat generation in the surface layer	2.5×10^{-6} (W/m^3)
$l(t)$	characteristic length scale	variable (m)
α	faulting dip angle	variable
x, z	horizontal × vertical distance	100,000 × 30,000 (m)
Δx, Δz	grid spacing	100 (m)
	starting depth for exhumation history	15,000 (m)
	thickness of lithosphere	100,000 (m)
v, u	velocity in x, z direction	variable (m/a)

6.1. Geometry

The two-dimensional finite difference grid with a horizontal distance x and a positive downwards distance z describes a cross-section parallel to the dip-slip movement of the normal fault with a variable dip angle. A variable velocity field with components u and v describes the exhumation of the footwall. In analogy to the suggested kinematics of the exhumation of metamorphic core complexes (e.g. Buck et al., 1988; van Wees et al., 1992), a footwall hinge line migration with an axial plane which migrates into the undeformed material was modelled (Fig. 8). Note that the angle γ_k between the surface and the axial plane and the angle γ between the axial plane and the fault remain equal and constant during the calculations. A chosen rock sample starts to exhume at a certain depth just beneath the fault plane with a temperature constrained by the initial geothermal gradient. During the calculations the variable velocity field in the footwall moves a chosen sample location to the surface.

6.2. Boundary conditions

Stüwe and Sandiford (1995) emphasised the problem of using a constant depth–constant heat flow lower boundary condition. In order to allow decoupling of strain in the mantle lithosphere they suggested to use a variable depth–constant heat flow or, even better, a variable depth–constant temperature lower boundary condition. However, in the presented calculations only the near-surface gradient and heat flow are investigated and therefore there is no need in modelling the temperature distribution within the whole lithosphere. To circumvent this problem only the upper 30 km of the lithosphere (i.e. the crust) are modelled and the change of the heat flow into the base of the crust is calculated analytically integrating the whole lithosphere (Mancktelow and Grasemann, 1997). This procedure results in a constant depth–variable heat flow lower boundary condition:

$$-k\frac{\mathrm{d}T}{\mathrm{d}z} = f(t)$$

where k is the conductivity, T the temperature and $f(t)$ a time-dependent function resulting from the analytical calculation. For the chosen initial temperature distribution and reasonable exhumation rates discussed below the initial heat flow at the Moho is 46 $\mathrm{mW/m^2}$ and after the period of rapid exhumation it is about 38 $\mathrm{mW/m^2}$. Note, that although the surface heat flow is increasing during rapid exhumation, the heat flow at depth has to drop, which is the direct consequence of using a constant-temperature variable-depth lower boundary condition at the base of the lithosphere. However, at the timescale observed (i.e. 5 Ma) the calculated geothermal gradient is insensitive to the lower boundary conditions and results from models assuming a basal constant heat flow or a constant temperature maintained at some fixed depth (i.e. variable heat flow) are indistinguishable (compare one-dimensional analytical solutions derived by Benfield, 1949 and Mancktelow and Grasemann, 1997).

The other boundary conditions are:

$$T = T_\mathrm{s} = 0$$

at the upper boundary where T_s is the constant surface temperature,

$$\frac{\mathrm{d}T}{\mathrm{d}x} = 0$$

at the left and right side.

6.3. Modelling procedure

After each time step the temperature and the location within the grid of a chosen sample location within the footwall is stored. From this record theoretical cooling curves are plotted and compared with the cooling history of the Rechnitz metamorphic core constrained by thermochronological methods (Fig. 9). Although this cooling curve is not tightly constrained it is clear that there was a period of faster cooling and probably exhumation somewhere around 20 Ma. As the starting depth of the chosen sample location is constrained by petrological observations and the sample has to exhume with such velocities that the thermochronological cooling history is reproduced, the only variable in the presented model is the *dip angle* and consequently the *displacement along the fault* and the *displacement velocity*. Five combinations of different faulting angles and faulting velocities were modelled (Table 3).

Table 3
Faulting angles, faulting velocities and total faulting distance which constrain the geometry of the presented numerical models

Model-run	Faulting angle (°)	Faulting velocity (m/a)	Total faulting distance (m)
1	10	0.0115	86,400
2	15	0.0077	58,000
3	20	0.0059	43,900
4	30	0.0040	30,000
5	50	0.0026	19,600

Note that in this table the faulting velocity represents the sum of the u and v component of the velocity field below the fault during the rapid exhumation of the footwall. After this period the near-surface heat flow at the base of the sediments is recorded and used for further calculations.

6.4. Discussion of assumptions

The purpose of this study is to quantify the surface heat flow above a normal fault using a mathematical model with a simplified geometry. Several models have been suggested for the exhumation of metamorphic core complexes. The proposed mechanisms are motion on low-angle faults (Wernicke, 1981) or rotation of high-angle normal faults (Buck et al., 1988; Wernicke and Axen, 1988). Partly these models require complex velocity fields in the footwall, fragmentation, rotation and sedimentary infill in the hanging wall, isostatic and flexural response to nor-

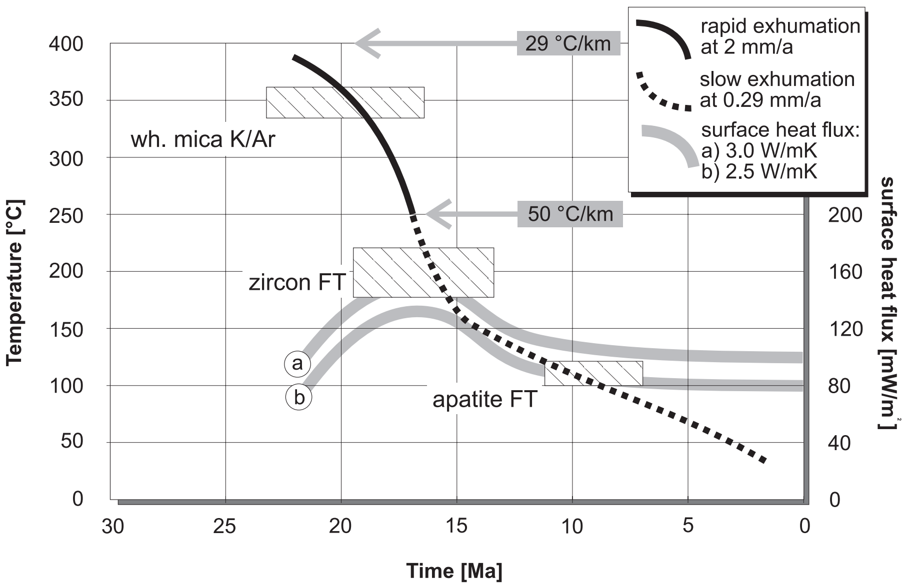

Fig. 9. Suggested temperature–time curve (i.e. cooling curve) for the exhumation of the Rechnitz Window. The solid curve indicates the period of exhumation at 2 mm/a whereas the dotted curve represents the subsequent slow exhumation (0.29 mm/a). Note that all parameter configurations used in this study have to result in this cooling pattern (thermochronological data taken from Dunkl and Demény, 1997). Additionally, the near-surface heat flow history is calculated for two models using a mean conductivity of 3.0 W m^{-1} K^{-1} (a) and 2.5 W m^{-1} K^{-1} (b), respectively. It is important to note that the maximum of these curves is exactly at the change from fast to slow exhumation.

mal faulting. These processes are not considered in the presented model and effects that influence the velocity field, and consequently the advection may result in under- or overestimation of the suggested results. However, the upper limit for the presented model is the heat flow constrained by the one-dimensional, analytical solution.

Frictional heating and fluid flow are neglected in the presented model. Frictional heating along a fault is a function of the applied shear stress and the slip rate (Carslaw and Jaeger, 1959). Although frictional heating might provide a planar heat source, if shear stress and extension rate are large, this effect is neglected because the magnitude of the shear stress acting on a fault is less known and may range from a few tens to a few hundreds of megapascals (England and Molnar, 1993). No account is taken of heat transfer by subsurface fluid flow, which is difficult to model and poorly understood (Bethke, 1989). During high tectonic activity, advection of heat is considered to be the first-order process controlling the overall heat budget (Sass et al., 1994).

6.5. Results

Based on the *PT* conditions of the footwall, the regional timing of extension and the thermochronologic data discussed above, the following conditions were used for the models 1–5. A chosen rock sample starts to be exhumed at 15 km depth just beneath the fault plane with a temperature of 377ºC. The initial temperature distribution was calculated analytically using the parameters in Table 2. The period of rapid faulting (i.e. exhumation rate of 2 mm/a of the footwall) starts at 22 Ma and lasts until 17 Ma. After that time the sample is at 5 km depth for all models and the footwall is exhumed with 0.29 mm/a to the surface.

Fig. 9 shows the calculated cooling curve (note that the samples from the footwall from all five models have to record the same cooling history) that fits the geochronological data. From the calculated model we have some additional information: the initial near-surface gradient at 22 Ma is about 29ºC/km and the surface heat flow is about 90 mW/m^2. After the period of rapid faulting at 17 Ma the gradient

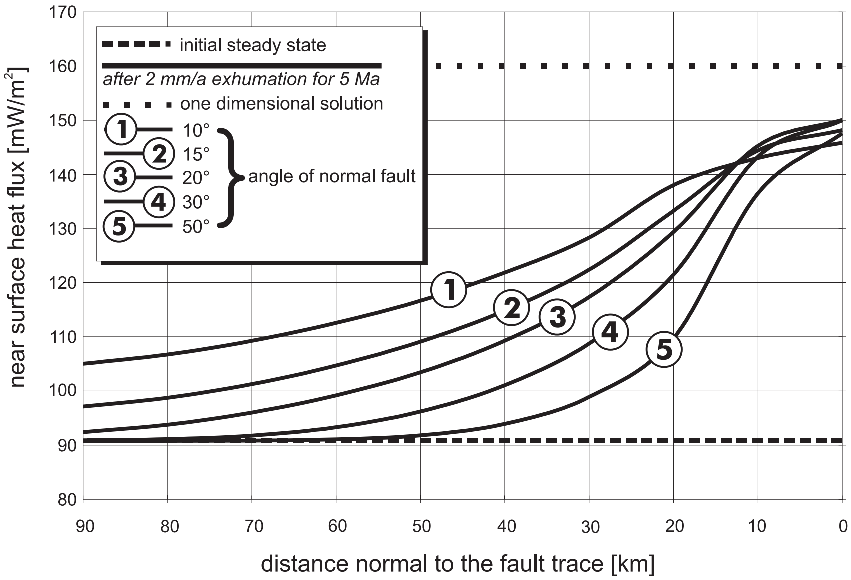

Fig. 10. Parameter map for models 1–5. The near-surface heat flow for a mean thermal conductivity of 3.0 W m^{-1} K^{-1} is plotted versus the distance to the fault trace. The dotted curve represents near-surface heat flow calculated with a one-dimensional analytical model neglecting the lateral heat conduction. The dashed curve indicates the initial near-surface heat flow. For further discussion see text. See Table 2 for physical parameters used for analytical and numerical calculations.

is dramatically elevated and about 50ºC/km. The surface heat flow at the fault trace depends on the fault angle but lies for all models between 145 and 150 mW/m^2. The change of the convex part of the curve to the concave part is not at the change of fast to slow faulting (at 17 Ma), but clearly after that period at about 15 Ma. This is due to the fact that the dramatically increased geothermal gradient relaxes after cessation of rapid movement, and consequently the sample continues to cool rapidly although the exhumation rate is nearly one order of magnitude less. In order to examine the influence of the period of rapid exhumation (i.e. 5 Ma at 2 mm/a) on the near-surface gradient, a parameter map (Fig. 10) showing the distance normal to the fault trace versus the heat flow in the hanging wall is plotted for the five models (i.e. 10º, 15º, 20º, 30º and 50º). The dashed line shows the initial near-surface heat flow of 90 mW/m^2 which is constant in the horizontal direction. The five solid curves show the horizontal distribution of the near-surface heat flow after the rapid faulting. It is clearly shown that within 8 km to the fault trace the near-surface heat flow in the hanging wall is for all models between 140 and 150 mW/m^2. The highest values are reached with 20–30º dip angles. This is due to the fact that in high-angle models the lateral cooling gradient is clearly larger, because 'hotter' material is displaced faster against 'colder' material. The width of the influence of the perturbation is strongly influenced by the dip angle: in a high-angle fault (e.g. 50º) the surface heat flow is only elevated at a distance of about 50 km to the fault trace. At locations beyond this distance the near-surface gradient is not influenced by the normal fault and the initial steady state value is preserved. Modelling a low-angle normal fault (e.g. <20º) this zone of near-surface thermal influence is more than the double distance (i.e. >100 km). This shows that the near-surface heat flow is clearly a function of the faulting geometry. A comparison of the model data with actual heat flow measurements normal to the trace of active extensional faults is suggested for further investigations.

The dotted line in Fig. 10 shows the result of a one-dimensional exhumation using the same model parameters, boundary and initial conditions but calculated with an analytical solution (Mancktelow and Grasemann, 1997). This comparison is useful because the one-dimensional solution constrains an upper limit for the near-surface heat flow calculated by the two-dimensional program. As a nature of one-dimensional calculations, the dip of the normal fault cannot be considered and therefore lateral heat conduction is neglected. Therefore, this solution places an upper limit to results with a more complex two-dimensional velocity field that would enhance lateral conduction of heat. It shows that such a simplification overestimates the heat flow of about 10 mW/m^2 at the fault, and in the order of 50 mW/m^2 at some distance to the fault trace compared with a two-dimensional approach.

It is important to note that the increased near-surface heat flow values of the presented models are recorded immediately after the period of normal faulting where the temperature distributions are mainly affected by advection of heat (second term on the right side in Eq. 1). After the period of rapid faulting other processes like conduction of heat or heat production (first and third term on the right side in Eq. 1) will control the change of temperatures with time. Therefore the presented results cannot be directly compared to recent heat flow measurement obtained by geophysical methods (Sass et al., 1994). For example, heat flow measurements from the metamorphic core complexes in the Basin and Range Province show a well-defined relative heat flow low (<80 mW/m^2). This distribution probably suggests that the transient elevated geothermal gradient caused initially by the exhumation of the metamorphic cores has largely relaxed and that the low heat flow might result from loss of the radioactivity as the upper crust attenuated (Lachenbruch et al., 1994).

7. Deduction of the palaeo-burial from vitrinite reflectance modelling

Increased heat flow alone is not sufficient to produce a high coal rank without the thermal blanketing of the sediment cover. To clarify the role of burial we modelled the coal maturation (see Fig. 11; the details are in Appendix C). The results are presented in Fig. 12. The diagram shows the relationship between the heat flow and burial depths. The minor difference between cases (A) and (B) proves, that sedimentation rate and the mode of cessation of the increased heat flow have a minor effect on the calculation of palaeo-burial. According to the numerical thermal modelling of the previous section the heat flow was 140–150 mW/m^2 near the fault in the hanging wall. Heat flow of this range can create the observed organic maturation with the blanketing effect of around 1100–1600 m of sediment.

Although the Sinnersdorf formation is preserved as small, thin remnants, the calculated palaeo-burial value seems to be realistic. The sedimentation rate was fast during Early–Middle Miocene time in the molasse basins of the Eastern Alps (foreland Molasse basin, Genser and Neubauer, 1996; Styrian basin, Ebner and Sachsenhofer, 1991a). In the Styrian basin the syn-rift sediment pile is as thick as 2 km in some subbasins. The isolated sediment remnants preserved as 'intramontane basins' in the area east of the Tauern Window indicate a former, much wider extent of the Neogene sediment cover (see Figs. 1 and 2). Erosion of the sediment sheet could have occurred (1) during the 'Styrian phase' which is a regional angular unconformity of Middle Miocene age, (2) during the early Pannonian erosional period ($\sim$10 Ma; Horváth, 1995), (3) and/or during the Pliocene erosional period ($\sim$5–2 Ma; Becker, 1993; Horváth and Cloetingh, 1996; see Fig. 11). The latest period is the most likely to be responsible for most of the erosion of the Sinnersdorf beds, because it was rather intense; it eroded the Neogene cover at the margin of the Pannonian basin from the Carpathian and Alpine foot-hills (Tari, 1994; Árkai et al., 1995; Frank et al., 1996). As the Rechnitz core complex is situated close to the margin of the Pannonian basin, this late flank-uplift has removed the former sediment cover of the surrounding of the core complex (Fig. 6).

8. Conclusions

During the formation of a metamorphic core complex the heat flow increases dramatically within the window as well as in the surrounding hanging wall. In case of the Rechnitz Window numerical thermal modelling suggests that the heat flow during extension reached the range of 140–150 mW/m^2 in the hanging wall at a distance <10 km of the window margin.

Apatite fission track data indicate that the period of increased temperature around the Rechnitz Window ended at around 13.6 ± 0.9 Ma.

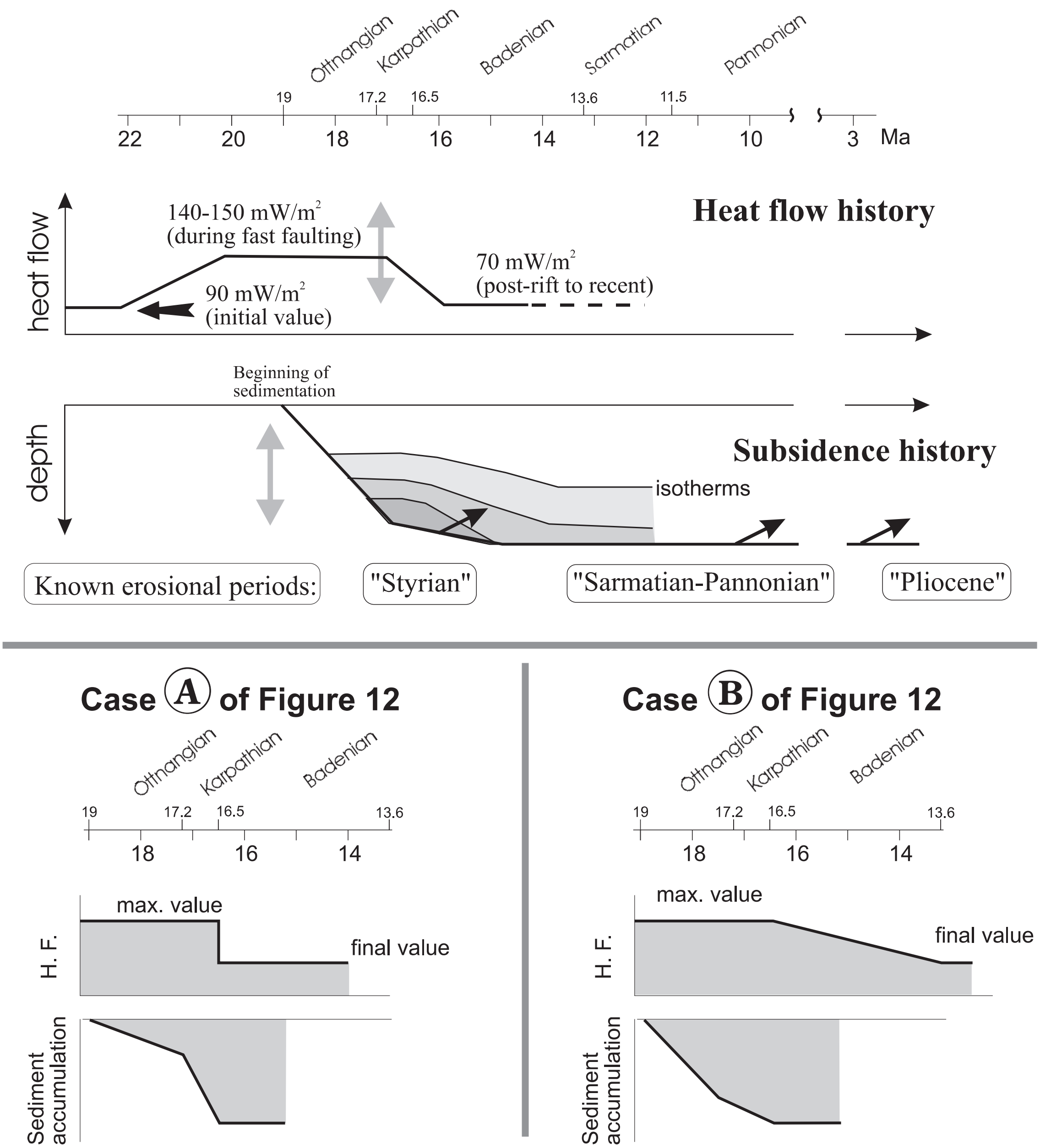

Fig. 11. Timing of the evolution of the sedimentary cover of the hanging wall. Such a scheme was used for the modelling of vitrinite reflectance. The constants of the modelling runs were: beginning of the sedimentation, thermal conductivity and the termination of the increased heat flow. The heat flow and the sediment thickness were the variables, represented by grey, symmetric arrows. Timescale according to Steininger et al. (1988). Cases (*A*) and (*B*) represent the most extreme, but possible conditions. *H.F.* = heat flow.

The tectonic denudation causing increased heat flow is alone capable of explaining the high coal rank of the Miocene syn-rift sediments. It is therefore not necessary to assume a hidden magmatic body as responsible heat source for the organic maturation and for the formation of epithermal stibnite mineralisation that occur in the Penninic rocks.

Based on numerical thermal modelling of the heat

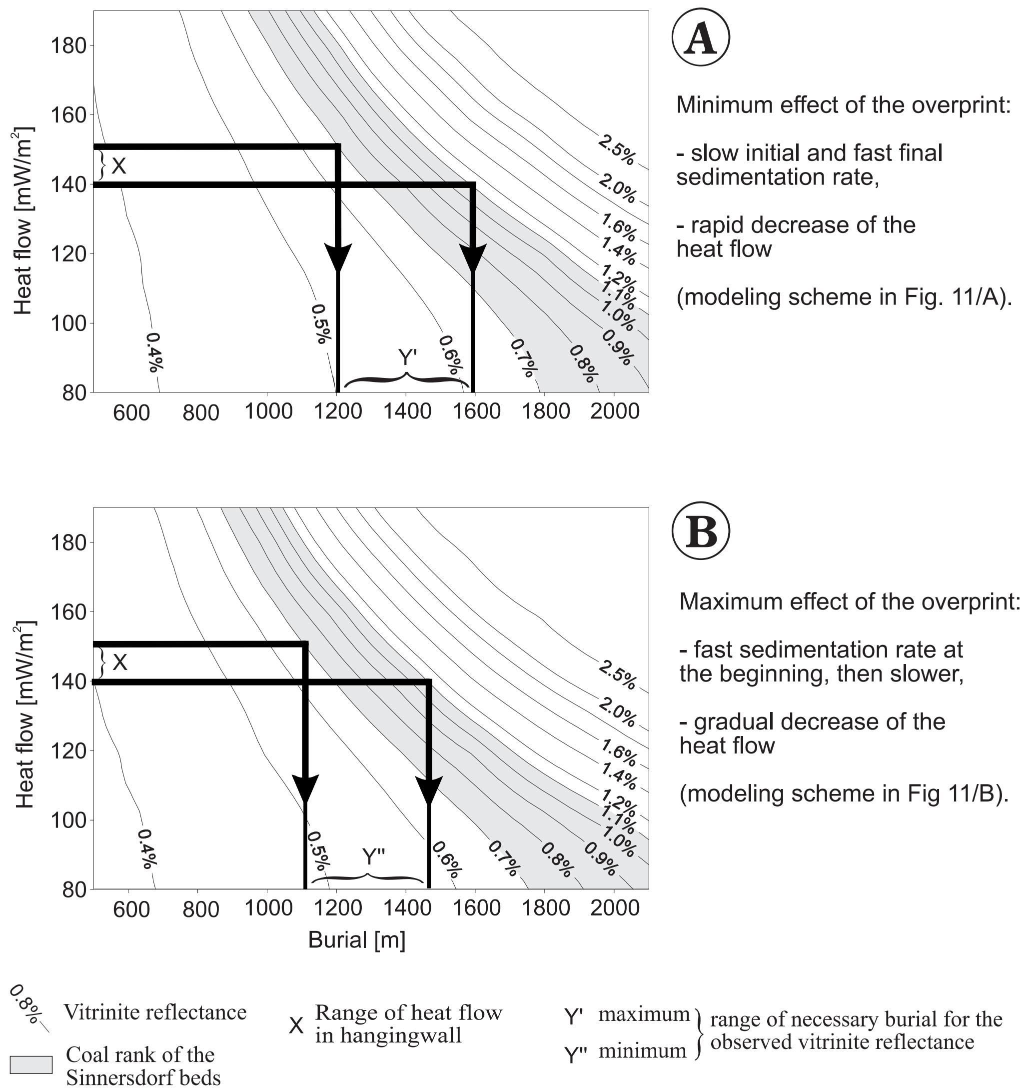

Fig. 12. Dependence of vitrinite reflectance upon heat flow and burial depth (details of modelling in Appendix C). The isolines of the two diagrams were constructed by fitting of the results of 88–88 modelling runs by different burial thickness and heat flow values (Fig. 11). In case (*A*) slow sedimentation rate is supposed at the beginning of the deposition, and rapid decrease of the heat flow at the end of Karpatian time. In case (*B*) fast initial sedimentation rate and prolonged thermal relaxation is supposed (see Fig. 11B).

flow and the vitrinite reflectance values we are able to elucidate the relationship between heat flow and burial depth. According to these considerations the burial of the presently exposed Sinnersdorf beds was in the order of 1100–1600 m.

The results of the modelling have a consequence on the evaluation of the hydrocarbon potential of deep, core complex-related sedimentary basins. If during tectonic denudation a deep (>1000 m) basin is forming and simultaneously filling with syn-rift sediments, then the thermal effect can produce extreme high organic maturation in the deepest part of the sediment sequence. Thus the estimation of the maturation of the deepest part of the basin from the maturation gradient detected in the higher part of the post-rift sequence may be erroneous and too low.

The syn-extension heating of the hanging wall could result in unexpectedly high maturation values.

Acknowledgements

The help of A. Pahr (Oberschützen) and F. Horváth (Budapest) during field work is gratefully acknowledged. Age standards were made available as a favour from C.W. Naeser (Denver) and A.J. Hurford (London). F. Grass (Vienna) helped with the irradiation of the samples. P. Dövényi (Budapest) suggested a typical value for the thermal conductivity of the Neogene sediments. The manuscript was improved by P. O'Shea (Tübingen). Discussions with R. Sachsenhofer (Leoben), L. Ratschbacher (Würzburg) and F. Koller (Vienna) — thanks for their valuable aid. The German Science Foundation financed the fission track part of this study in the frame of the Collaborative Research Centre 275. Support from the Hungarian National Scientific Research Fund (OTKA Project No. 232/91) is also acknowledged. B.G. developed the used computer software with funding from project P-11765-GEO of the Austrian Fond zur Förderung der wissenschaftlichen Forschung. Constructive reviews by B. Wernicke and B.E. John were much appreciated and improved both content and style.

Appendix A. Sample preparation, FT dating

Conglomerate and sandstone samples were investigated from the northeastern margin of the Styrian basin. Representative samples from the coarse conglomerate were made by combination of pieces from 50 cobbles. The petrographical composition of the pebbles are gneiss and micaschist varieties, originated dominantly from the Grobgneiss unit. The samples were treated by the common heavy liquid and magnetic separation processes. For fission track age determinations the apatite crystals were embedded in epoxy resin, the zircons in FEP-Teflon. For apatite 1% nitric acid was used with 2.5–3 min etching time (Burchart, 1972). In the case of zircon crystals, the eutectic melt of NaOH–KOH was used at the temperature of 200ºC. Neutron irradiations were made at the reactor of the Nuclear Institute of the Austrian Universities (Vienna). The external detector method was used (Gleadow, 1981), after irradiation the induced fission tracks in the mica detectors were etched by 40% HF for 40 min. Track counts were made with a Zeiss NU 2 microscope, with magnification of 1600×.

The FT ages were determined by the zeta method (Hurford and Green, 1983) using zircon from the Fish Canyon Tuff, Buluk Member Tuff and Tardree Rhyolite and apatite from Durango and Fish Canyon Tuff. Reference ages of 27.8 ± 0.2 Ma for the Fish Canyon Tuff, 31.4 ± 0.5 Ma for Durango apatite, 16.2 ± 0.6 Ma for Buluk Member Tuff and 58.7 ± 1.1 Ma for Tardree Rhyolite has been adopted according to Hurford and Green (1983), Hurford and Hammerschmidt (1985), Green (1985) and Hurford and Watkins (1987). The error was calculated by using the classical procedure, i.e. by the double Poisson dispersion (Green, 1985).

Appendix B. Numerical heat flow modelling

The time-dependent heat transfer equation in two dimensions including heat conduction, advection and production but for incompressible conditions is:

$$\frac{\partial T}{\partial t} = \kappa \left(\frac{\partial^2 T}{\partial x^2} + \frac{\partial^2 T}{\partial z^2} \right) + \left(u \frac{\partial T}{\partial x} + v \frac{\partial T}{\partial z} \right) + \frac{A(z,t)}{\rho C} \tag{1}$$

where: T = temperature; (ºC); t = time (s); κ = thermal diffusivity (m^2/s); x, z = horizontal and vertical (i.e. depth) direction (m); u,v = velocities in x and z direction (m/s); $A(z,t)$ = volumetric heat production (W/m^3); C = specific heat (J kg^{-1} K^{-1}); ρ = density (kg/m^3).

In the presented model the volumetric heat production is not a constant value but an exponential function where the heat generation decays with depth:

$$A(z,t) = A_0 \exp\left(\frac{-z}{l(t)} \right) \tag{2}$$

where A_0 is the heat generation in the surface layer, $l(t)$ is the variable depth that changes with time at which the heat production drops to 1/e of this surface value. This procedure allows to erode the radioactive layer during exhumation, leading to a steady decrease in the surface heat production with time. The numerical calculations are solved over a equally spaced grid with 1000 × 300 nodes describing the temperature distribution over a horizontal distance of 100 km and a vertical distance of 30 km. This system is solved numerically in two dimensions using an ADI (alternating-direction-implicit) method with a two-step scheme (Peaceman and Rachford, 1955). However, the advection term has to be solved separately using an upwind differencing scheme (which applies backward or forward differencing depending on the sign of the velocity vector. This procedure is only stable as long as:

$$\Delta t \leq \left\{ \frac{|u|}{\Delta x} + \frac{|v|}{\Delta z} + \frac{2\kappa}{(\Delta z)^2} \right\}^{-1}$$

Appendix C. Modelling of the vitrinite reflectance

The modelling of organic maturation was done according to the Lopatin method. There are four variables, one constant, and the output is the vitrinite reflectance (Fig. 11).

(a) *Heat flow*. As the maximum value was 150 mW/m^2 according to the modelling of the exhumation, we modelled the organic maturation in the range of 70–200 mW/m^2 in steps of 10 and 20 mW/m^2 to produce a wide window to trace the relation of different factors.

(b) *Thickness*. The range of the burial of the syn-rift sediments varied between 200 and 2200 m.

(c) *Decreasing rate of the heat flow after its maximum*. Several possibilities were tested between very rapid drop of heat flow in Karpatian time (16.5 Ma) and slow, gradual decrease until the end of the Badenian stage (13.6 Ma). Both of these two extremes fit to the geological facts. The rapid faulting has terminated in Karpatian time (this gives the argument for a high heat flow value until 16.5 Ma); on the other hand low vitrinite reflectance in Badenian and Sarmatian sediments proves diminished heat flow at that time (Sachsenhofer, 1994).

(d) *Sedimentation rate*. This has also some effect on the organic maturation. Faster sedimentation produces higher coal rank than slow sedimentation (with identical heat flow and total thickness of the sediment sequence).

We considered the thermal conductivity of the sediments to be constant. The empirical value determined on the Neogene sediments of the Pannonian basin of 2.3 W m^{-1} K^{-1} was used (Dövényi and Horváth, 1988; P. Dövényi, pers. commun.). It is clear that the conductivity is changing during burial, but the effect of its shift is insignificant for our calculation.

Based on the results of the vitrinite reflectance modelling several plots were designed showing the dependence of iso-maturation lines on heat flow and burial. Fig. 12 presents the two most extreme cases. Fig. 12A shows the vitrinite maturity values when a sudden drop of the heat flow from the maximum to the final value occurred at 16.5 Ma and the Ottnangian sediment sequence is half as thick as the Karpatian one (see also Fig. 11A). Fig. 12B shows the maturation trend in case of a long-lasting gradual decrease of the heat flow until the end of the Badenian stage, and faster initial sedimentation (Ottnangian sediments are twice as thick as the Karpatian pile; see Fig. 11B). These conditions result in the maximum possible maturation. Thus, shallower burial is sufficient to reach the observed coal maturation than in case A).

References

Aric, K., Gutdeutsch, R., Klinger, G., Lenhardt, W., 1987. Seismological studies in the Eastern Alps. In: Flügel, H.W., Faupl, P. (Eds.), Geodynamics of the Eastern Alps. Deuticke, Wien, pp. 325–333.

Árkai, P., Balogh, K., Dunkl, I., 1995. Timing of low-temperature metamorphism and cooling of the Paleozoic and Mesozoic formations of the Bükkium, innermost Western Carpathians, Hungary. Geol. Rundsch. 84, 334–344.

Bartley, J.M., Fletcher, J.M., Glazner, A.F., 1990. Tertiary extension and contraction of lower-plate rocks in the central Mojave metamorphic core complex, southern California. Tectonics 9, 521–534.

Becker, A., 1993. Contemporary state of stress and neotectonic deformation in the Carpathian–Pannonian region. Terra Nova 5, 375–388.

Belocky, R., Sachsenhofer, R.F., Pohl, W., 1991. Neue Argumente für eine miozäne epithermale Genese der Antimonerzlagerstätte Schlaining (Burgenland/Österreich): Flüssigkeitseinschlußuntersuchungen und das Inkohlungsbild der benachbarten Tertiärbecken. Berg- Hüttenmänn. Monatsh. 136, 209–213.

Benfield, A.E., 1949. A problem of the temperature distribution in a moving medium. Q. Appl. Math. 6, 439–443.

Bethke, C.M., 1989. Modeling subsurface flow in sedimentary basins. Geol. Rundsch. 78, 129–154.

Blanckenburg, F., Villa, I.M., Baur, H., Morteani, G., Steiger, R.H., 1989. Time calibration of a PT-path from the Western Tauern Window, Eastern Alps: the problem of closure temperatures. Contrib. Mineral. Petrol. 101, 1–11.

Buck, W.R., 1993. Effect of lithospheric thickness on the formation of high- and low-angle normal faults. Geology 21, 933–936.

Buck, W.R., Martinez, F., Steckler, M.S., Cochran, J.R., 1988. Thermal consequences of lithospheric extension: pure and simple. Tectonics 7, 213–234.

Burchart, J., 1972. Fission track age determinations of accessory apatite from the Tatra Mountains, Poland. Earth Planet. Sci. Lett. 15, 418–422.

Carslaw, S., Jaeger, J.C., 1959. Conduction of Heat in Solids. Oxford University Press, New York, 510 pp.

Cliff, R.A., Droop, G.T.R., Rex, D.C., 1985. Alpine metamorphism in south-east Tauern Window, Austria, 2. Rates of heating, cooling and uplift. J. Metamorph. Geol. 3, 403–415.

Davis, G.A., Lister, G.S., 1986. Detachment faulting in continental extension; Perspectives from the Southwestern U.S. Cordillera. In: Clark, S.P., Burchfiel, B.C., Suppe, J. (Eds.), Processes in Continental Lithospheric Deformation. Special Paper — Geological Society of America, 218, Boulder, CO, pp. 133–159.

Decker, K., Peresson, H., 1996. Tertiary kinematics in the Alpine–Carpathian–Pannonian system: links between thrusting, transform faulting and crustal extension. In: Wessely, G., Liebl, W. (Eds.), Oil and Gas in Alpidic Thrust Belts and Basins of Central and Eastern Europe. EAGE London, Spec. Publ. 5, 69–77.

Dokka, R.K., 1993. Original dip and subsequent modification of a Cordilleran detachment fault, Mojave extensional belt, California. Geology 21, 711–714.

Dokka, R.K., Mahaffie, M.J., Snoke, A.W., 1986. Thermochronologic evidence of major tectonic denudation associated with detachment faulting, northern Ruby Mountains, East Humboldt Range, Nevada. Tectonics 5, 995–1006.

Dövényi, P., Horváth, F., 1988. A review of temperature, thermal conductivity, and heat flow data from the Pannonian Basin. In: Royden, L.H., Horváth, F. (Eds.), The Pannonian Basin — a Study in Basin Evolution. Am. Assoc. Pet. Geol. Mem. 45, 235–255.

Dunkl, I., 1992. Final episodes of the cooling history of eastern termination of the Alps. In: Neubauer, F. (Ed.), Geological

Evolution of the Internal Eastern Alps and Carpathians and of the Pannonian Basin (ALCAPA): Field Guide, University of Graz, Graz, pp. 137–139.

Dunkl, I., Demény, A., 1997. Exhumation of the Rechnitz Window at the border of Eastern Alps and Pannonian basin during Neogene extension. Tectonophysics 272, 197–211.

Ebner, F., Sachsenhofer, R.F., 1991a. Die Entwicklungsgeschichte des Steirischen Tertiärbeckens. Mitt. Abt. Geol. Paläontol. Landesmus. Joanneum 49, 1–96.

Ebner, F., Sachsenhofer, R.F., 1991b. Paleogeography, subsidence and thermal history of the Neogene Syrian basin (Pannonian basin system, Austria). Tectonophysics 242, 133–150.

England, P., Molnar, P., 1993. The interpretation of inverted metamorphic isograds using simple physical calculations. Tectonics 12, 145–157.

Fayon, A.K., Stump, E., Peacock, S.M., 1996. Thermal structure and resetting of apatite fission-track ages in the hanging wall of detachment faults. Abstract Volume of Int. Workshop on Fission-track Dating, Gent, p. 33.

Flügel, H.W., 1988. Steirisches Becken–Südburgenländische Schwelle; geologische Karte des prätertiären Untergrundes 1 : 200,000. Geologische Bundesanstalt, Wien.

Flügel, H.W., Neubauer, F., 1984. Geologische Karte der Steiermark 1 : 200.000. Mitt. Abt. Geol. Paläontol. Landesmus. Joanneum 45.

Frank, W., Lelkes-Felvári, Gy., Dunkl, I., 1996. Thermal history of Austroalpine basement rocks of the borehole Fertörákos-1004. In: Dudich, E., Lobitzer, H. (Eds.), Advances in Austrian–Hungarian Joint Geological Research, Geological Institute of Hungary, Budapest, pp. 177–195.

Fülöp, J., Dank, V. (Eds.), 1987. Pre-Tertiary basement map of Hungary. 1 : 500,000. Hungarian Geological Survey, Budapest.

Genser, J., Neubauer, F., 1996. Subsidenzentwicklung des Österreichischen Molassebeckens: Aussagen über die alpine Orogenese. Symposium Tektonik, Strukturgeologie, Kristallingeologie 6, Salzburg, pp. 147–150.

Gleadow, A.J.W., 1981. Fission-track dating methods: what are the real alternatives? Nuclear Tracks 5, 3–14.

Grasemann, B., Mancktelow, N., 1993. Two-dimensional thermal modeling of normal faulting: the Simplon Fault Zone, Central Alps, Switzerland. Tectonophysics 225, 155–165.

Green, P.F., 1985. Comparison of zeta calibration baselines for fission-track dating of apatite, zircon and sphene. Chem. Geol. 58, 1–22.

Grum, W., Frimmel, H.E., Koller, F., 1992. Sr-Isotope and whole rock geochemical studies on the genesis of the stibnite deposit Schlaining (Penninic unit, Eastern Alps). Mitt. Ges. Geol. Bergbaustud. Österr. 38, 73–92.

Herrmann, P., Pahr, A., 1988. Geologische Karte der Republik Österreich, 1 : 50000, Erläuterungen zu Blatt 138 Rechnitz. Geologische Bundesanstalt, Wien, 40 pp.

Horváth, F., 1985. Thickness of Neogene–Quaternary basin fill of the Pannonian Basin System. 1 : 1,000,000. Am. Assoc. Pet. Geol. Mem. 45, Map 8.

Horváth, F., 1995. Phases of compression during the evolution of the Pannonian Basin and its bearing on hydrocarbon exploration. Mar. Pet. Geol. 12, 837–844.

Horváth, F., Cloetingh, S., 1996. Stress-induced late-stage subsidence anomalies in the Pannonian basin. Tectonophysics 266, 287–300.

House, M.A., Hodges, M.A., 1994. Limits on the tectonic significance of rapid cooling events in extensional settings: insights from the Bitterroot metamorphic core complex, Idaho, Montana. Geology 22, 1007–1010.

Hurford, A.J., Green, P.F., 1983. The zeta age calibration of fission-track dating. Chem. Geol. (Isot. Geosci. Sect.) 41, 285–312.

Hurford, A.J., Hammerschmidt, K., 1985. $^{40}Ar/^{39}Ar$ and K/Ar dating of the Bishop an Fish Canyon Tuffs: calibration ages for fission track dating standards. Chem. Geol. (Isot. Geosci. Sect.) 58, 23–32.

Hurford, A.J., Watkins, R.T., 1987. Fission-track age of the tuffs of the Buluk Member, Bakate Formation, Northern Kenya: a suitable fission-track age standard. Chem. Geol. 66, 209–216.

Hurford, A.J., Fitch, F.J., Clarke, A., 1984. Resolution of the age structure of the detrital zircon populations of two Lower Cretaceous sandstones from the Weald of England by fission track dating. Geol. Mag. 121, 269–277.

Inger, S., Cliff, R.A., 1994. Timing of metamorphism in the Tauern Window, Eastern Alps: Rb–Sr ages and fabric formation. J. Metamorph. Geol. 12, 695–707.

John, B.E., 1987. Geometry and evolution of a mid-crustal extensional fault system: Chemehuevi Mountains, southeastern California. In: Coward, M.P., Dewey, J.F., Hancock, P.L. (Eds.), Continental Extensional Tectonics. Geol. Soc. London Spec. Publ. 28, 313–335.

John, B.E., Foster, D.A., 1993. Structural and thermal constraints on the initiation angle of detachment faulting in the southern Basin and Range: the Chemehuevi Mountains case study. Geol. Soc. Am. Bull. 105, 1091–1108.

Ketcham, R.A., 1996. Thermal models of core-complex evolution in Arizona and New Guinea: implications for ancient cooling paths and present day flow. Tectonics 15, 933–951.

Koller, F., 1985. Petrologie und Geochemie der Ophiolite des Penninikums am Alpenostrand. Jahrb. Geol. Bundesanst. 128, 83–150.

Lachenbruch, A.H., Sass, J.H., Morgan, P., 1994. Thermal regime of the southern Basin and Range Province, 2. Implications of heat flow for regional extension and metamorphic core complexes. J. Geophys. Res. B99 (11), 22121–22133.

Mancktelow, N., Grasemann, B., 1997. Time-dependent effects of heat advection and topography on cooling histories during erosion. Tectonophysics 270, 167–195.

Müller, W., Dallmeyer, R.D., Neubauer, F., Thöni, M., 1992. Chronology of Variscan metamorphic events and low grade Alpine overprint in the eastern Lower Austroalpine Units: Rb/Sr and $^{40}Ar/^{39}Ar$ age data (Wechsel and Raabalpenunit, Eastern Alps). Terra Abstr. 4 (2), 46.

Neubauer, F., Genser, J., 1990. Architektur und Kinematik der östlichen Zentralalpen — eine Übersicht. Mitt. Naturwiss. Ver. Steiermark 120, 203–219.

Pahr, A., 1980. Die Fenster von Rechnitz, Berstein und Moltern. In: Oberhauser, R. (Ed.), Der Geologische Aufbau Österreichs. Springer, Vienna, pp. 320–326.

Pahr, A., 1984. Geologische Karte der Republik Österreich, 1 : 50,000, Erläuterungen zu Blatt 137 Oberwart. Geologische Bundesanstalt, Wien, 47 pp.

Peaceman, D.W., Rachford, H.H., 1955. The numerical solution of parabolic and elliptic differential equations. J. Indian Math. Soc. 3, 28–41.

Ratschbacher, L., Frisch, W., Neubauer, F., Schmid, S.M., Neugebauer, J., 1989. Extension in compressional orogenic belts: the Eastern Alps. Geology 17, 404–407.

Ratschbacher, L., Behrmann, J.H., Pahr, A., 1990. Penninic windows at the eastern end of the Alps and their relation to the intra-Carpathian basins. Tectonophysics 172, 91–105.

Ratschbacher, L., Frisch, W., Linzer, H.G., Merle, O., 1991. Lateral extrusion in the Eastern Alps, part 2. Structural analysis. Tectonics 10, 257–271.

Reynolds, S.J., Lister, G.S., 1990. Folding of mylonitic zones in Cordilleran metamorphic core complexes: evidence from near the mylonitic front. Geology 18, 216–219.

Royden, L.H., Horváth, F., Rumpler, J., 1983. Evolution of the Pannonian basin system, 1. Tectonics. Tectonics 2, 63–90.

Ruppel, C., Royden, L., Hodges, K.V., 1988. Thermal modeling of extensional tectonics: application to pressure–temperature–time histories of metamorphic rocks. Tectonics 7, 947–957.

Sachsenhofer, R.F., 1990. Eine Inkohlungskarte des Steirischen Tertiärbeckens. Mitt. Naturwiss. Ver. Steiermark 120, 251–264.

Sachsenhofer, R.F., 1991. Maturität im Steirischen Tertiärbecken. Erdöl Erdgas Kohle 107, 12–17.

Sachsenhofer, R.F., 1992. Coalification and thermal histories of Tertiary basins in relation to late Alpidic evolution of the Eastern Alps. Geol. Rundsch. 81, 291–308.

Sachsenhofer, R.F., 1994. Petroleum generation and migration in the Styrian Basin (Pannonian Basin system, Austria): an integrated geochemical and numerical modeling study. Mar. Pet. Geol. 11, 684–701.

Sass, J.H., Lachenbruch, A.H., Galanis Jr., S.P., Morgan, P., Priest, S.S., Moses Jr., T.H., Munroe, R.J., 1994. Thermal regime of the southern Basin and Range Province, 1. Heat flow data from Arizona and the Mojave Desert of California and Nevada. J. Geophys. Res. B99 (11), 22093–22119.

Schönlaub, H.P., 1973. Schwamm-Spiculae aus dem Rechnitzer Schifergebirge und ihr stratigraphischer Wert. Jahrb. Geol. Bundesanst. 116, 35–48.

Steininger, F.F., Müller, C., Rögl, F., 1988. Correlation of Central Paratethys, Eastern Paratethys, and Mediterranean Neogene stages. Am. Assoc. Pet. Geol. Mem. 45, 79–88.

Stüwe, K., Sandiford, M., 1995. Mantle–lithospheric deformation and crustal metamorphism with some speculations on the thermal and mechanical significance of the Tauern Event, Eastern Alps. Tectonophysics 242, 115–132.

Tari, G., 1994. Alpine Tectonics of the Pannonian Basin. Ph.D. Thesis, Rice University, Houston, TX, 501 pp.

Tari, G., Horváth, F., 1995. Middle Miocene extensional collapse in the Alpine–Pannonian transition zone. In: Horváth, F., Tari, G., Bokor, Cs. (Eds.), Extensional Collapse of the Alpine Orogene and Hydrocarbon Prospects in the Basement and Basin Fill of the Western Pannonian Basin. AAPG Int. Conf., Nice, Guideb. to Fieldtrip 6, pp. 75–105.

Tari, G., Horváth, F., Weir, G., 1995. Palinspastic reconstruction of the Alpine/Carpathian/Pannonian system. In: Horváth, F., Tari, G., Bokor, Cs. (Eds.), Extensional Collapse of the Alpine Orogen and Hydrocarbon Prospects in the Basement and Basin Fill of the Western Pannonian Basin. AAPG Int. Conf., Nice, Guideb. to Fieldtrip 6, pp. 119–132.

Van Wees, J.D., de Jong, K., Cloetingh, S., 1992. Two-dimensional P–T–t modelling and the dynamics of extension and inversion in the Betic Zone (SE Spain). Tectonophysics 203, 305–324.

Wernicke, B., 1981. Low-angle normal faults in the Basin and Range Province — nappe tectonics in an extending orogen. Nature 291, 645–648.

Wernicke, B., Axen, G.A., 1988. On the role of isostasy in the evolution of normal fault systems. Geology 16, 848–851.

Zimmermann, R., Hammerschmidt, K., Franz, G., 1994. Eocene high pressure metamorphism in the Penninic units of the Tauern Window (Eastern Alps): evidence from ^{40}Ar–^{39}Ar dating and petrological investigations. Contrib. Mineral. Petrol. 117, 175–186.